Negative refractive index in coaxial plasmon waveguides

René de Waele,[1,*] Stanley P. Burgos,[2] Harry A. Atwater,[2] and Albert Polman[1]

[1]*Center for Nanophotonics, FOM-Institute for Atomic and Molecular Physics (AMOLF), Science Park 104, 1098 XG Amsterdam, The Netherlands*

[2]*California Institute of Technology, 1200 East California Boulevard, Pasadena, California 91125, USA*

**waele@amolf.nl*

Abstract: We theoretically show that coaxial waveguides composed of a metallic core, surrounded by a dielectric cylinder and clad by a metal outer layer exhibit negative refractive index modes over a broad spectral range in the visible. For narrow dielectric gaps (10 nm GaP embedded in Ag) a figure-of-merit of 18 can be achieved at $\lambda_0 = 460$ nm. For larger dielectric gaps the negative index spectral range extends well below the surface plasmon resonance frequency. By fine-tuning the coaxial geometry the special case of $n = -1$ at a figure-of-merit of 5, or $n = 0$ for a decay length of 500 nm can be achieved.

OCIS codes: (240.6680) Optics at surfaces; (160.3918) Metamaterials; (222.0220) Optical design and fabrication.

References and links

1. W. L. Barnes, A. Dereux, and T. W. Ebbesen, "Surface plasmon subwavelength optics," Nature **424**, 824–830 (2003).
2. E. Ozbay, "Plasmonics: Merging photonics and electronics at nanoscale dimensions," Science **311**, 189–193 (2006).
3. J. Weeber, M. U. González, A. L. Baudrion, and A. Dereux, "Surface plasmon routing along right angle bent metal strips," Appl. Phys. Lett. **87**, 221101 (2005).
4. A. Drezet, F. R. Aussenegg, A. Leitner, and J. R. Krenn, "Dielectric stripes on gold as surface plasmon waveguides," Appl. Phys. Lett. **88**, 094104 (2006).
5. P. Berini, "Plasmon polariton modes guided by a metal film of finite width," Opt. Lett. **24**, 1011–1013 (1999).
6. M. Sandtke and L. Kuipers, "Slow guided surface plasmons at telecom frequencies," Nat. Phot. **1**, 573–576 (2007).
7. M. I. Stockman, "Nanofocusing of optical energy in tapered plasmonic waveguides," Phys. Rev. Lett. **93**, 137404 (2004).
8. E. Verhagen, A. Polman, and L. Kuipers, "Nanofocusing in laterally tapered plasmonic waveguides," Opt. Express **16**, 45–57 (2008).
9. J. A. Dionne, L. A. Sweatlock, H. A. Atwater, and A. Polman, "Plasmon slot waveguides: Towards chip-scale propagation with subwavelength-scale localization," Phys. Rev. B **73**, 035407 (2006).
10. H. Miyazaki and Y. Kurokawa, "Squeezing visible light waves into a 3-nm-thick and 55-nm-long plasmon cavity," Phys. Rev. Lett. **96**, 097401 (2006).
11. H. J. Lezec, J. A. Dionne, and H. A. Atwater, "Negative refraction at visible frequencies," Science **316**, 430–432 (2007).
12. G. Shvets, "Photonic approach to making a material with a negative index of refraction," Phys. Rev. B **67**, 035109 (2003).
13. J. A. Dionne, E. Verhagen, A. Polman, and H. A. Atwater, "Are negative index materials achievable with surface plasmon waveguides? a case study of three plasmonic geometries," Opt. Express **16**, 19001–19017 (2008).

#126829 - $15.00 USD Received 12 Apr 2010; accepted 14 May 2010; published 28 May 2010

14. W. J. Fan, S. Zhang, B. Minhas, K. J. Malloy, and S. R. J. Brueck, "Enhanced infrared transmission through subwavelength coaxial metallic arrays," Phys. Rev. Lett. **94**, 033902 (2005).
15. F. I. Baida, A. Belkhir, D. V. Labeke, and O. Lamrous, "Subwavelength metallic coaxial waveguides in the optical range: Role of the plasmonic modes," Phys. Rev. B **74**, 205419 (2006).
16. R. de Waele, S. P. Burgos, A. Polman, and H. A. Atwater, "Plasmon dispersion in coaxial waveguides from single-cavity optical transmission measurements," Nano Lett. **9**, 2832–2837 (2009).
17. J. B. Pendry, "Negative refraction makes a perfect lens," Phys. Rev. Lett. **85**, 3966–3969 (2000).
18. D. R. Smith, J. B. Pendry, and M. C. K. Wiltshire, "Metamaterials and negative refractive index," Science **305**, 788–792 (2004).
19. G. Dolling, C. Enkrich, M. Wegener, C. M. Soukoulis, and S. Linden, "Simultaneous negative phase and group velocity of light in a metamaterial," Science **312**, 892–894 (2006).
20. V. M. Shalaev, "Optical negative-index metamaterials," Nat. Photon. **1**, 41–48 (2007).
21. J. Valentine, S. Zhang, T. Zentgraf, E. Ulin-Avila, D. Genov, G. Bartal, and X. Zhang, "Three-dimensional optical metamaterial with a negative refractive index," Nature **455**, 376–379 (2008).
22. S. P. Burgos, R. de Waele, A. Polman, and H. A. Atwater, "A single-layer wide-angle negative index metamaterial at visible frequencies," Nat. Mater. **9**, 407–412 (2010).
23. G. Dolling, M. Wegener, and S. Linden, "Realization of a three-functional-layer negative-index photonic metamaterial," Opt. Lett. **32**, 551–553 (2007).
24. P. B. Johnson and R. W. Christy, "Optical constants of the noble metals," Phys. Rev. B **6**, 4370–4379 (1972).
25. E. Palik, ed., *Handbook of optical constants of solids* (Academic Press, Inc., Orlando, FL., 1985).
26. A. Alù, M. G. Silveirinha, A. Salandrino, and N. Engheta, "Epsilon-near-zero metamaterials and electromagnetic sources: Tailoring the radiation phase pattern," Phys. Rev. B **75**, 155410 (2007).
27. M. Meier and A. Wokaun, "Enhanced fields on large metal particles: dynamic depolarization," Opt. Lett. **8**, 581–583 (1983).
28. Z. Jacob, L. V. Alekseyev, and E. Narimanov, "Optical hyperlens: Far-field imaging beyond the diffraction limit," Opt. Express **14**, 8247–8256 (2006).

1. Introduction

Controlling the propagation of light at the nanoscale is one of the challenges in photonics. Surface plasmons, electromagnetic modes that propagate at a metal/dielectric interface provide a key opportunity to achieve this goal, due to their relatively small evanescent fields [1, 2]. Moreover, as their dispersion can be strongly controlled by geometry, their effective wavelength can be shrunk well below the free-space wavelength, enabling further miniaturization of optical components. Initial experiments on plasmon optics were carried out at planar metal/dielectric interfaces, demonstrating basic control of plasmons. Plasmonic components such as mirrors [3, 4] and waveguides [5, 6] were realized, however still of relatively large size due to the > 100 nm evanescent tails, and with limited control over dispersion. Subsequently, insulator-metal-insulator structures were investigated, and have demonstrated confinement of light to < 100 nm length scales in taper geometries [7, 8], though at high loss. The reverse, metal-insulator-metal (MIM) geometries, have demonstrated lower loss, higher dispersion [9, 10], and recently the attainment of a negative index of refraction [11–13].

A disadvantage of planar MIM structures is that they only confine light in one transverse direction. Recently, coaxial MIM waveguides, composed of a metal core surrounded by a dielectric cylinder clad by a metal outer layer have been introduced, that confine light in all transverse directions [14, 15]. We have recently reported optical transmission measurements through single coaxial waveguides, from which the dispersion diagram for these nanoscale waveguides was determined [16].

Inspired by the earlier work on MIM waveguides, a natural question arises whether coaxial waveguides would posses a negative refractive index, and if so, for what geometry and over what spectral range. Since the coaxial waveguides are essentially 3-dimensional objects, the observation of negative index in individual coaxes, also inspires the design of 3-dimensional negative-index metamaterials [17–21] composed of arrays of coaxial waveguides [22].

Here, we theoretically study the dispersion of coaxial Ag/Si/Ag plasmon waveguides and demonstrate that for well-chosen geometries modes with a negative refractive index are ob-

#126829 - $15.00 USD Received 12 Apr 2010; accepted 14 May 2010; published 28 May 2010

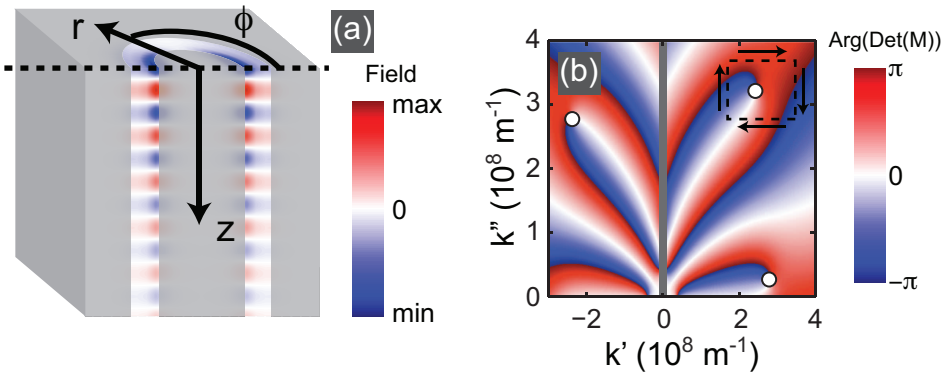

Fig. 1. Coaxial plasmon waveguide geometry and numerical mode solving method. (a) Schematic cross-section of a coaxial waveguide with the definition of the cylindrical polar coordinates, r, ϕ and z. The metallic inner core and outer cladding separate a dielectric channel. A schematic wave propagating in the waveguide in the direction of positive z is also indicated. (b) Argument θ of the determinant, $\det[M(k)]$, plotted in the complex k-plane for a Ag/Si/Ag waveguide with 75 nm inner core diameter and 10-nm-wide dielectric channel at $\omega = 3 \times 10^{15}$ rad/s. By cycling around the closed loop indicated by the dashed square the net number of discontinuities in θ is determined. Zero positions are indicated by the white circles.

served. These modes are dominant over other waveguide modes for a wide range of frequencies above the surface plasmon resonance frequency. We discuss the influence of waveguide geometry and material on the mode index and demonstrate that the figure-of-merit (FOM), defined as the magnitude of the real part of the propagation constant in the waveguide divided by the imaginary part [13, 23], can be as high as 18.

2. Method

The azimuthal dependence of the fields is described by the harmonic function $e^{in\phi}$ of order n. In the remainder we only consider modes with $n = 1$, since these are the lowest order modes that couple to free-space radiation. The radial dependence of the fields in all three domains (metal-dielectric-metal) is described by solutions to the 2^{nd} order Bessel differential equation. We apply a Bessel function of the first kind, J_n, to the metal core, as that function remains finite at the waveguide axis. A Hankel function of the first kind, $H_n^{(1)}$, is applied to the metal cladding. Inside the dielectric channel the radial field is described by two linearly independent cylinder functions. The arguments of the cylinder functions in each of the three domains is $\kappa_i r$, where κ_i is the radial wave number in medium i, defined via

$$\kappa_i^2 \equiv \varepsilon_i \frac{\omega^2}{c^2} - k^2 \tag{1}$$

where ε_i is the complex dielectric constant in domain i. To satisfy the condition that fields decay to zero at radial infinity we take the square root of Eq. (1) such that the radial wave number has a positive imaginary part.

On each domain boundary we formulate four continuity conditions for the tangential components of the electric and magnetic fields. The optical eigenmodes of the coaxial waveguide are found when the determinant of the resulting homogeneous system of eight equations with eight unknown coefficients vanishes,

$$\det[M(k)] = 0 \tag{2}$$

#126829 - $15.00 USD Received 12 Apr 2010; accepted 14 May 2010; published 28 May 2010

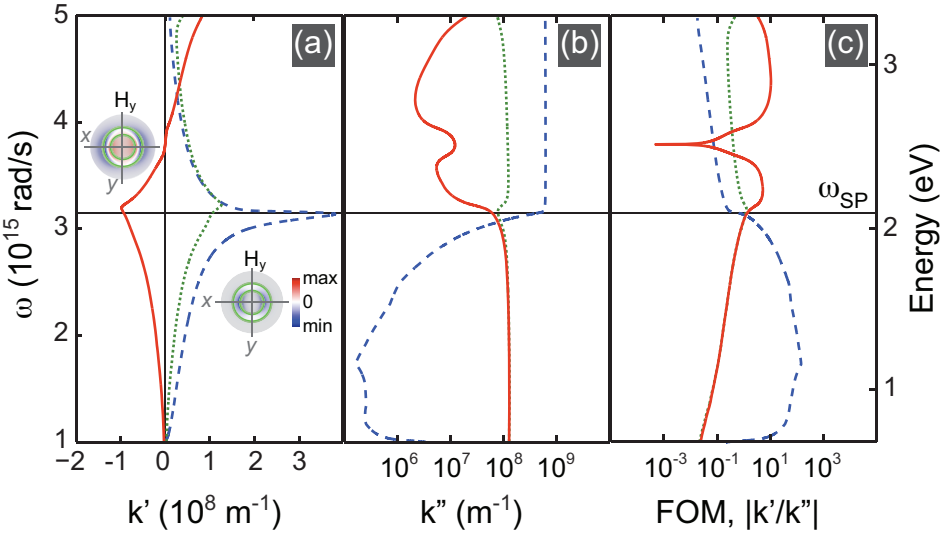

Fig. 2. Dispersion relations of the three lowest-order modes of a coaxial waveguide with 75-nm-diameter Ag core, 25-nm wide Si channel, and infinite outer Ag cladding. Radial frequency is plotted versus propagation constant k' (a), attenuation constant k'' (b), and figure-of-merit k'/k'' (c). The Ag/Si surface plasmon resonance frequency $\omega_{SP} = 3.15 \times 10^{15}$ rad/s ($\lambda_0 = 598$ nm) is indicated by the horizontal line. Panel (a) shows two modes with positive index (blue dashed curve and green dotted curve) and one mode with a negative index below a frequency of $\sim 3.8 \times 10^{15}$ rad/s (red drawn curve). The insets in (a) show the H_y field distribution in the transverse plane of the waveguide at 2.8×10^{15} rad/s for the positive-index mode (blue dashed dispersion curve) and at 3.6×10^{15} rad/s for the negative-index mode.

where M is the matrix of the system of equations. We have used two independent methods for determining the optical modes, $k(\omega)$, of the structure. One involved a numerical procedure developed to detect local minima of the determinant of the system in the complex k-plane. The other method relies on the fact that the argument, θ, given by

$$\det[M(k)] = |\det[M(k)]|e^{i\theta} \tag{3}$$

is undefined when $\det[M(k)] = 0$. This can be visualized in a plot of θ in the complex k-plane. An example is shown in Fig. 1(b) where θ is plotted for a coaxial waveguide with a Ag core and cladding and a 10 nm silicon spacer layer. We used empirically determined optical constants for the metal [24] and dielectric [25]. Contour lines in the figure appear to close in on each other at each of the zeros, which are indicated by the white dots in the figure. By counting each discontinuity $-\pi \rightarrow \pi$ and $\pi \rightarrow -\pi$ about a closed loop in the figure [for an example, see the dashed square loop in Fig. 1(b)] we are able to determine the number of zeros in the enclosed area. In case we find that one or more zeros reside in the area, we split the area up in smaller pieces and repeat the procedure until the location of the zero(s) is determined with double computer precision.

Using this method, solutions for k were found for real frequency, so that dispersion relations, $\omega(k)$, could be constructed. Calculations were performed in the optical angular frequency regime 1×10^{15} rad/s $< \omega < 5 \times 10^{15}$ rad/s (free-space wavelength, $\lambda_0 = 377$–1884 nm). We only consider modes with positive energy velocity, v_e, or equivalently, positive attenuation constant k'' [13]. Therefore, to achieve antiparallel energy and phase velocity, which is the unique

#126829 - $15.00 USD
Received 12 Apr 2010; accepted 14 May 2010; published 28 May 2010

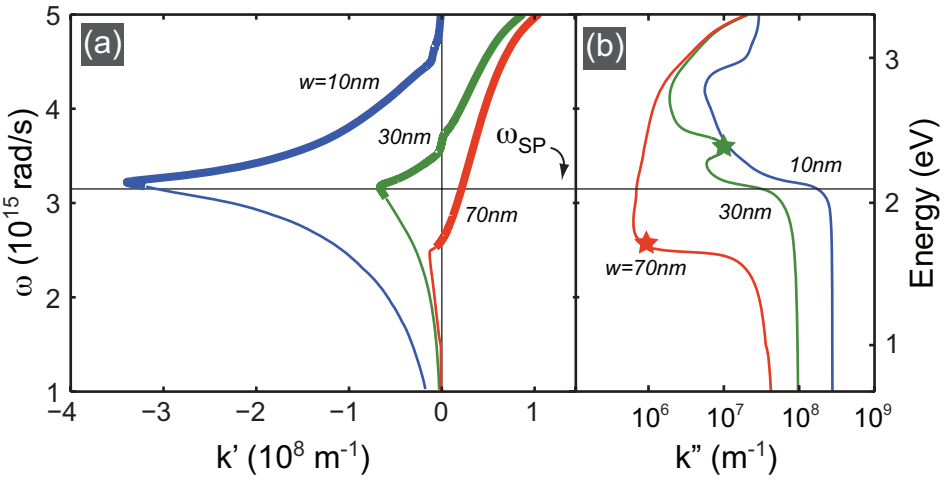

Fig. 3. Dispersion relations for negative-index coaxial waveguides with Ag core and cladding and Si dielectric channel, (a): $\omega(k')$; (b): $\omega(k'')$. The inner core diameter is fixed at 75 nm and the Si-channel thickness w is 10 nm, 30 nm, and 70 nm. Positive-index modes [as shown in Fig. 2(a)] are not shown in the figure. The bold sections of the dispersion curves indicate the spectral range over which the negative-index mode is dominant, i.e. has lower loss than the positive index modes. The frequency where the red and green dispersion curves cross $k' = 0$ is indicated by the star-symbols.

requirement for a negative mode index, the propagation constant k' needs to be negative.

3. Results

Figure 2 shows the dispersion relation, $\omega(k)$, for the three lowest-order modes in a coaxial waveguide consisting of a 75-nm-diameter Ag core surrounded by a 25-nm-thick Si layer and infinite Ag cladding. In (a) the angular frequency is plotted against k', while (b) shows the frequency as function of k'', which determines the propagation length of light in the waveguide via

$$L = \frac{1}{2k''}. \tag{4}$$

The surface plasmon resonance frequency $\omega_{SP} = 3.15 \times 10^{15}$ rad/s ($\lambda_0 = 598$ nm) is indicated by the horizontal line.

Figure 2(a) shows two coaxial modes (blue dashed line and green dotted line) with positive propagation constants over the entire spectral range. Both dispersion curves closely resemble the dispersion of a surface plasmon polariton propagating along a planar Si/Ag interface. However, the corresponding propagation constants [Fig. 2(a)], are nearly three times as large as for the planar single interface plasmon. This is due to the fact that confinement of the plasmon in the coaxial waveguide geometry leads to larger mode overlap with the metal. Figure 2(a) also shows the existence of a third mode (red drawn curve) that has a negative propagation constant k' for frequencies below 3.8×10^{15} rad/s ($\lambda_0 = 496$ nm). The effective index $n = ck'/\omega$ ranges from $-9 < n < 5$ in the frequency range of Fig. 2. The insets in (a) show the H_y field in the transverse plane for the negative-index mode (calculated at $\omega = 3.6 \times 10^{15}$ rad/s) as well as for the most dispersive positive mode (blue dashed curve in Fig. 2(a), $\omega = 2.8 \times 10^{15}$ rad/s). From the images it is clear that the mode with positive effective index has a symmetric field distribution with respect to the two centers of the dielectric channel on the x-axis. The H_y field is primarily

#126829 - $15.00 USD
Received 12 Apr 2010; accepted 14 May 2010; published 28 May 2010

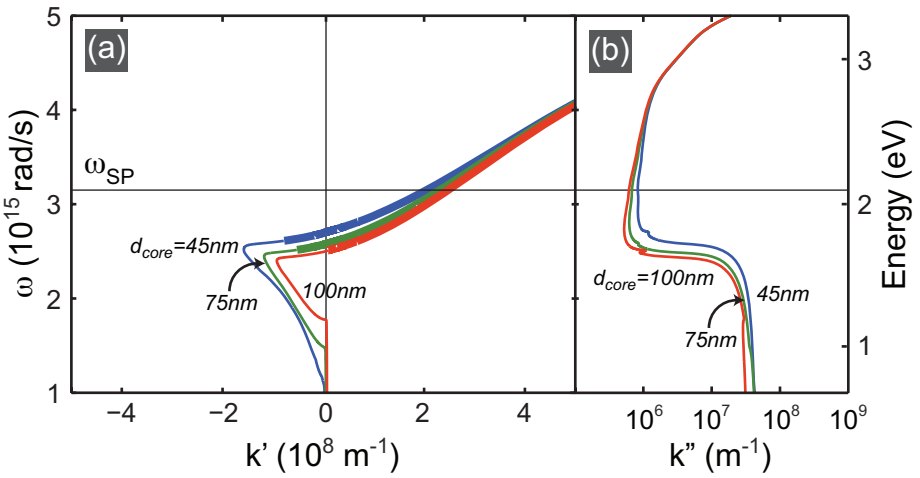

Fig. 4. Dispersion relations for coaxial waveguides with Ag core and cladding and 70-nm-wide Si dielectric channel, (a): $\omega(k')$; (b): $\omega(k'')$. The inner core diameter, d_{core}, is 45 nm (blue curves), 75 nm (green curves) and 100 nm (red curves). Only modes with negative index are plotted. Bold lines indicate the spectral range where the mode is dominant over the positive-index mode.

concentrated at the boundary between the metal core and dielectric channel. The negative-index mode in contrast, has its field primarily concentrated at the outermost channel boundary and has an H_y-field distribution that is anti-symmetric about the center of the dielectric channel, similar to modes with negative index in planar metal-insulator-metal waveguides [13].

Figure 2(b) shows that for frequencies below the surface plasmon resonance frequency ω_{SP} the lowest-order positive-index mode (blue dashed line) has lowest loss and will therefore be dominant over other modes. Interestingly, above ω_{SP} the negative-index mode (red curve) becomes the dominant mode, as its losses are significantly lower than those for the positive-index modes. Figure 2(c) shows the figure-of-merit (FOM), k'/k'', of the modes. As can be seen, the negative-index mode has a FOM that approaches 10 for a narrow frequency interval around 3.4×10^{15} rad/s ($\lambda_0 = 554$ nm). The data in Fig. 2 clearly demonstrate that dominant modes of negative index indeed exist in coaxial plasmon waveguides.

Next, we investigate the conditions that are required to achieve a negative index by varying the geometry and materials of the waveguide. Figure 3 shows the effect of changing the dielectric layer thickness on the dispersion of the negative index mode. Calculations were performed for a Ag/Si/Ag coaxial waveguide with a core diameter of 75 nm for a dielectric layer thickness of 10 nm, 30 nm, and 70 nm. Figure 3(a) shows that the variation in dielectric layer thickness has a very dramatic effect on the dispersion of the negative-index mode. First of all, the largest negative index is observed for the thinnest dielectric. Second, while for the 10-nm and 30-nm dielectric gaps the frequency of the resonance associated with the negative index mode appears close to the surface plasmon resonance at 3.2×10^{15} rad/s, for the 70-nm gap this resonance is significantly red-shifted to 2.5×10^{15} rad/s. The spectral range over which the mode is dominant, indicated by the bold curves in Fig. 3(a), also extends to lower frequencies when increasing the channel width. For the 70-nm gaps a narrow frequency range is found near 2.4×10^{15} rad/s ($\lambda_0 = 785$ nm) where the index is negative and the figure-of-merit is 5.

As the dispersion branches cross the $k' = 0$ line the effective refractive index of the mode vanishes [26]. Coaxial waveguides with a narrow dielectric gap suffer high loss at this frequency. The green star in Fig. 3(b) indicates the frequency at which the dispersion curve crosses the

#126829 - $15.00 USD Received 12 Apr 2010; accepted 14 May 2010; published 28 May 2010

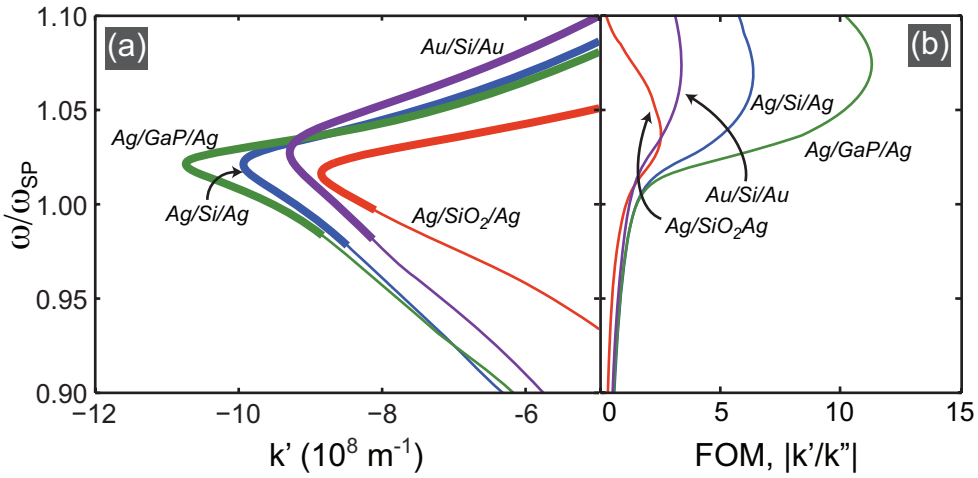

Fig. 5. Dispersion relations for coaxial waveguides with 75-nm-diameter metal core, 25-nm-wide dielectric channel and infinite metal cladding, (a): $\omega(k')$; (b): FOM k'/k''. The type of metal in the core and cladding, as well as the dielectric material was varied. The frequency axes are normalized to the corresponding surface plasmon resonance frequency ω_{SP}. Blue curves are for a Si channel surrounded by Ag ($\omega_{SP} = 3.15 \times 10^{15}$ rad/s), green curves for GaP in Ag ($\omega_{SP} = 3.49 \times 10^{15}$ rad/s), red curves for SiO_2 in Ag ($\omega_{SP} = 5.24 \times 10^{15}$ rad/s) and purple curves for Si in Au ($\omega_{SP} = 2.77 \times 10^{15}$ rad/s). Bold curves indicate the spectral range where the negative-index mode is dominant.

$k' = 0$ line for the 30-nm gap; a high value of $k'' = 10^7$ m^{-1} is found. In contrast, for the 70-nm-wide dielectric channel waveguides the losses at the $k' = 0$ crossing [red star in Fig. 3(b)] are much lower ($k'' < 10^6$ m^{-1}), corresponding to a decay length of 500 nm. Note that in the spectral range where the phase velocity ω/k' goes to zero, the group velocity, $v_g = d\omega/dk'$, is much larger than zero.

The two striking effects observed here: a) waveguide resonances that shift with geometry, and b) increased propagation length for $k' = 0$ modes for increasing dielectric thickness are in strong contrast to what is observed in planar metal-insulator-metal waveguides [13]. This suggests that coupling of plasmon fields across the nanoscale diameter of the metal core strongly influences the dispersion of the negative index modes. To investigate this, we studied the influence of the metal core diameter on the dispersion of the mode, while keeping the channel width fixed to 70 nm. Figure 4 shows the results for waveguides with inner core diameters of 45, 75 and 100 nm. The figure shows that the spectral range where the mode is both dominant and characterized by a negative index becomes smaller going from a 45-nm-diameter core to a 75 nm core, and vanishes when the core size is increased to 100 nm. This behavior coincides with a red-shift of the resonance in k'' when the core diameter is increased [Fig. 4(b)]. We attribute the resonance red-shift for increasing core diameter to a depolarization effect similar to what is known for bulk metallic particles, which show a plasmon resonance red-shift for increasing diameter [27]. Based on this insight, we predict that a large degree of control over dispersion and resonance red-shift may also be attained in planar structures composed of a multi-layered stack of metal and dielectric. In fact, negative index materials based on metal-dielectric multi-layers have been reported in literature [28]. A final observation that can be made in Fig. 4 regards the special case of $n = -1$; for a coaxial waveguide with a core diameter of 50 nm and a 70-nm wide Si channel a mode with n$= -1$ is observed with a FOM$= 5$ at $\omega = 2.61 \times 10^{15}$ rad/s (free-space wavelength of 720 nm).

#126829 - $15.00 USD
Received 12 Apr 2010; accepted 14 May 2010; published 28 May 2010

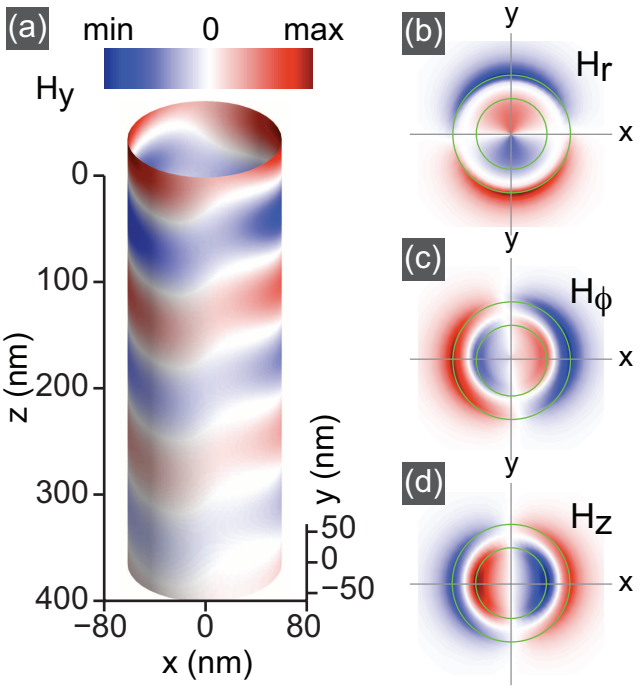

Fig. 6. Magnetic field images of a coaxial waveguide with 75 nm Ag core diameter, 25-nm-wide GaP-filled ring and infinite Ag cladding at a frequency of 3.75×10^{15} rad/s. In (a) we plot the H_y field distribution on the boundary of the Ag cladding with the dielectric channel. Note that the phase-fronts in the waveguide are in general not perpendicular to the optical axis (z-axis). In (b-d) we plot the polar magnetic field components in the transverse plane. The amplitude of the fields plotted in the figure has the same order of magnitude in all of the four panels.

Thus far we have studied the influence of the coax geometry on the frequency dispersion of k. Next, we will investigate the effect of changing the type of metal in core and cladding, as well as the dielectric in the cylindrical channel. Figure 5 shows the frequency dispersion for a coaxial waveguide with inner metal core diameter of 75 nm and dielectric channel width of 25 nm surrounded by an infinite metal cladding. We compare the results for Si (blue curves), GaP (green curves), and silica (red curves) channels in Ag, and for a Si channel in Au (purple curves). The curves are normalized to the surface plasmon resonance frequency for the corresponding planar metal/dielectric geometry. Interestingly, coaxial plasmon waveguides support dominant negative index modes regardless of the investigated choice of materials. The propagation vector k' is most strongly negative for waveguides filled with GaP and least negative for silica, which indicates that, to obtain a strong effect, the dielectric constant needs to be high ($n_{GaP} = 3.5$ at the GaP/Ag surface plasmon resonance). The figure-of-merit for the modes in Fig. 5(a) is plotted in Fig. 5(b). Due to the low loss and high index of GaP, the highest figure-of-merit is found in these waveguides. The highest number we found (FOM = 18) was for a 10-nm-wide GaP channel in Ag at $\omega = 4.1 \times 10^{15}$ rad/s ($\lambda_0 = 460$ nm, data not shown). Waveguides composed of Au show a lower FOM than those with Ag, which is attributed to the higher losses in Au.

Finally, in Fig. 6 we present the field distribution in a coaxial waveguide with negative index. Figure 6(a) shows the H_y-field on the outer metal-dielectric interface of a coaxial waveguide with 75-nm-diameter Ag core and 25-nm-wide GaP channel for a frequency $\omega = 3.75 \times 10^{15}$

#126829 - $15.00 USD
Received 12 Apr 2010; accepted 14 May 2010; published 28 May 2010

rad/s (free-space wavelength of 500 nm, $\omega/\omega_{SP} = 1.08$ in Fig. 5). Clearly, the phase fronts in the waveguide are not planar. As a result, a non-zero z-component of the electromagnetic field is observed. Figure 6(b) shows the distribution of H_r in the transverse plane. Its magnitude is similar to that of the H_y-field. For completeness, Figs. 6(c) and 6(d) show the H_ϕ and H_z components of the field. Note that these fields are antisymmetric with respect to the center of the dielectric channel and are located mostly inside the metal.

4. Conclusion

We have theoretically demonstrated that coaxial plasmon waveguides sustain modes with negative refractive index at optical frequencies. The negative-index modes have a larger propagation length than the positive-index modes over a large spectral range, depending on the dielectric thickness. For a 10-nm-wide GaP dielectric and a 75-nm-wide Ag core a figure-of-merit $k'/k'' = 18$ is found at $\lambda_0 = 460$ nm. For Ag/Si/Ag coaxial waveguides with increasing Si-channel thickness the dominant negative-index mode shifts well below the surface plasmon resonance frequency: for a 70 nm Si-channel it is found at $\lambda_0 = 750$ nm. The mode index can be fine-tuned to a value of -1 with a figure-of-merit as high as 5 at 720 nm. At slightly higher frequencies, the same mode has an effective index n=0 with positive group velocity, and a decay length of 500 nm. Overall higher tunability and figure-of-merit are found for coaxial waveguides of Ag rather than Au, and filled with a dielectric of highest optical constant. Based on the large degree of dispersion control that can be achieved with coaxial plasmon waveguides we anticipate that these structures will find use in new designs for nanoscale photonic integrated circuits (waveguides, splitters, multiplexers), in three-dimensional negative-index metamaterials, and invisibility cloaks.

#126829 - $15.00 USD Received 12 Apr 2010; accepted 14 May 2010; published 28 May 2010